

Effects of chemical composition and thermohaline mixing on the accreting components for low-mass close binaries: application to blue stragglers

Xuefei Chen^{1,2}★ and Zhanwen Han¹

¹ National Astronomical Observatories/Yunnan Observatory, CAS, Kunming, 650011, P.R.China

² Graduate School of the Chinese Academy of Sciences

17 December 2018

ABSTRACT

Blue stragglers (BSs) are important objects in cluster populations because of their peculiar properties. The colours and magnitudes of these objects are critical parameters in population synthesis of the host cluster and may depend remarkably on BSs' surface composition. Observations show that some BSs are short-orbital-period binaries, which may be accounted for by mass transfer in low-mass binaries. We therefore studied the effects of surface composition and thermohaline mixing caused by secular instability on the accreting components for low-mass binaries and applied the results on a short-orbital-period BS F190 in the old cluster M67.

We examine thermohaline mixing in a low-mass accreting-main-sequence star and find that, except the redistribution of composition under the surface, the mixing affects the accretor very little during Roche lobe overflow unless thermohaline mixing is treated as an instantaneous process. A series of calculations are then carried out for low-mass binaries under different assumptions. The results indicate no distinction in surface composition between the models with and without thermohaline mixing during Roche lobe overflow, but we still see the divergences of evolutionary tracks on Hertzsprung-Russell diagram and colour-magnitude diagram. The change of surface composition makes the gainer bluer and smaller than the ones with original surface composition while thermohaline mixing lessens the effect slightly. If thermohaline mixing were to act instantaneously, the effect would be lessened more. Our calculation shows that case A and case B mass transfer may produce BSs in short- or relatively short-orbital-period binaries (including Algol systems), and that CNO abundance abnormalities could be observed in these products. This is consistent with the results of Monte-Carlo simulations by previous studies.

Our simulation of F190 shows that the primary's mass M_{1i} of the appropriate models is located in the range of 1.40 to $1.45M_{\odot}$ with initial mass ratio $q_i = 1.5$ and initial orbital period $P_i = 0.8$ days, indicating that case A is a more likely evolutionary channel than case B to form this object. The simulation also shows that it is very likely that F190 is still in a slow stage of mass transfer. As a consequence, obvious CNO abundance abnormalities should be observed for the object.

Key words: binaries:close -stars:evolution - stars:blue straggler

1 INTRODUCTION

Blue stragglers (BSs), which have stayed on the main sequence for a time exceeding that expected from standard stellar evolution theory for their masses, are important in population synthesis because of their peculiar properties. These objects lie above and blueward of the turn-off in the

colour-magnitude diagram (CMD) of a cluster, may contribute remarkably spectral energy in the blue and ultraviolet, and affect the integrated spectrum of the host clusters as they are bright and blue (Deng et al. 1999). The characters of BSs, i.e. luminosity, temperature, gravity etc., are relevant to their formation mechanism. There are various possible origins for BSs in theory, i.e. close-binary evolution (mass transfer from a companion or coalescence of both companions), stellar collisions (single-single, binary-single and

★ xuefeichen717@hotmail.com

binary-binary), interior mixing, recent star formation etc. (Stryker 1993). Given the diversity of BSs within one cluster, it is likely that more than one formation mechanisms play a role (Leonard 1996). Observational evidence shows that binaries are at least important in some cluster BSs and in some field BSs (Carney et al. 2001; Leonard & Peter 1996; Milone & Latham 1992; Peterson, Carney & Latham 1984; Stryker 1993).

Since the binary mass-exchange hypothesis was originally advanced by McCrea (1964) to explain the BS phenomenon, a number of attempts have been made to test the hypothesis in open clusters (Collier & Jenkins 1984; Pols & Marinus 1994; Hurley et al. 2001). However there is a lack of detailed binary evolution calculations. Monte-Carlo simulations (Collier & Jenkins 1984; Pols & Marinus 1994) show that binary coalescence via case A evolution (mass transfer begins when the primary is on the main sequence) may be an important source of BSs in some clusters while case B evolution (mass transfer begins when the primary is in Hertzsprung gap) can only account for BSs in short-orbital-period binaries. Meanwhile, case A may also produce BSs by stable mass transfer as it does not always or immediately lead to a merger. The difficulty in verifying the binary mass transfer hypothesis is the lack of evidence for variations of radial velocities for most BSs. However some BSs have already been confirmed to be in binaries. A typical example is F190, a single-lined spectroscopic binary with a 4.2 days period (Milone & Latham 1992) in the old open cluster M67. As well, IUE (International Ultraviolet Explorer) spectra (Landsman et al. 1998) provide evidence that F90 and F131 (in M67) are Algol-type mass transfer systems. With the improvement of observational means, more and more BSs are detected to have variations in radial velocity. It is therefore necessary to study the hypothesis in detail. As more hydrogen is mixed into the center of an accretor which is still on the main sequence at the onset of Roche lobe overflow (RLOF), the accreting component goes upwards along the main sequence in response to accretion and its time on the main sequence is extended. When the mass of the accretor is more massive than the corresponding cluster turn-off mass at the age of the cluster, it may be recognized as a BS and show element contamination from the primary on the surface. The element contamination will effect observational characteristics of the star and it is dependent on the details of the accretion process.

Evolution of close binaries has been well studied over the last decades (see a review of van den Heuvel (1994) and some recent papers by de loore & Vanbeveren (1995), Marks & Sarna (1998), Han et al. (2000), Hurley, Tout & Pols (2002) and Nelson & Eggleton (2001) etc.). Many of these works are related to the secondary (initially lower mass component in a binary), where accretion mode and accretion rate are concerned on. Since the accreting matter may be originally in the convective core of the primary, thermohaline mixing, which results from accreting material with a higher molecular weight than the surface layers, was first introduced by Ulrich (1972) to describe this effect (see also Kippenhan, Ruschenplatt & Thomas (1980)). It was treated as an instantaneous process in intermediate-mass and massive close binaries for its short time scale in these systems by some authors (Hellings 1984; de Loore & Vanbeveren 1994; de Loore & Vanbeveren 1995). As well, the details of accretion process

during RLOF were ignored in these studies, and we have no knowledge of the effect of composition of secondaries during RLOF. Wellstein, Langer & Braun (2001) treated thermohaline mixing in a time-dependent way in massive binary evolution and argued that this is important as both thermohaline mixing and accretion occur on a thermal timescale. In this paper, we concentrate on the behavior of secondaries in low-mass binaries during or just ceasing RLOF, applying the results on short-orbital-period BSs. The computations are introduced in section 2 and thermohaline mixing for low-mass close binaries is examined in section 3. The results are shown in section 4. In section 5, we show a best model of F190 by simulation in a complete parameter space. Finally we give our conclusions, discussions and outlook on the work.

2 COMPUTATIONS

We use the stellar evolution code devised by Eggleton (1971; 1972; 1973) and updated with the latest physics over the last three decades (Han et al. 1994; Pols et al. 1995; Pols et al. 1998). The ROLF is included via the boundary condition

$$\frac{dm}{dt} = C \cdot \text{Max}[0, (\frac{r_{\text{star}}}{r_{\text{lobe}}} - 1)^3], \quad (1)$$

when we follow the evolution of the mass donor. Here dm/dt is the mass loss rate of the primary, r_{star} is the radius of the star, r_{lobe} is the radius of its Roche lobe and C is a constant. Here we take $C = 500 M_{\odot} \text{yr}^{-1}$ so that RLOF can proceed steadily and the lobe-filling star overfills its Roche lobe as necessary but never overfills it by much, i.e. a transfer rate of $5 \times 10^{-7} M_{\odot} \text{yr}^{-1}$ corresponding to an overfill of 0.1 per cent. When following the evolution of the primary, we store its mass-loss history as an input in subsequent calculations of the secondary, including the age when RLOF begins, mass loss rate, and the composition of the lost matter. The calculation of the secondary is stopped as it overfills its Roche lobe and the system becomes a contact binary. Contact binaries are beyond our considerations here for there are many uncertainties during contact phase. Merger models will be studied in another paper.

The accreting matter is assumed to be deposited onto the surface of the secondary with zero falling velocity and distributed homogeneously all over the outer layers. The change of chemical composition on the secondary's surface caused by the accreting matter is

$$(\frac{\partial X_i}{\partial t}) = \frac{(\partial M / \partial t)}{(\partial M / \partial t)dt + M_s} (X_{ia} - X_{is}) \quad (2)$$

where $\partial M / \partial t$ is the mass accretion rate, X_{ia} and X_{is} are element abundances of the accreting matter and of the secondary's surface for species i , respectively. M_s is the mass of outer most layer of the secondary. M_s will change with the moving of non-Lagrangian mesh as well as the chosen resolution, but it is so small ($\sim 10^{-9} - 10^{-12} M_{\odot}$) in comparison with $(\partial M / \partial t)dt$ ($\sim 10^{-3} - 10^{-5} M_{\odot}$) during RLOF that we can ignore the effect of various M_s on element abundances. Before and after RLOF, we get $\partial X_i / \partial t = 0$ from the equation, which is reasonable in the absence of mixing.

The opacity table is from OPAL (Iglesias & Rogers 1996) with solar composition and from Alexander & Ferguson (1994a; 1994b) in our calculations. Only stable RLOFs

are considered in our calculations, under which the accreting component may completely accrete the matter lost by the primary as mass transfer is very slow in this case ($\sim 10^{-9} M_{\odot} \text{yr}^{-1}$, see section 4). The mass and angular momentum of the systems are therefore assumed to be conservative. Convective overshooting has little effect in the mass range($1.0\text{--}1.6 M_{\odot}$) we considered (Chen & Han 2003). We, therefore, have not considered it in our calculations.

3 SECULAR INSTABILITY AND THEMOMHALINE MIXING

During mass transfer in a close binary, the accreting matter may be originally in the convective core of the donor. It is rich in helium relative to the gainer's surface and has a higher mean molecular weight, which will cause secular instability during or after accretion. Thermohaline mixing will occur in this case. Kippehahn, Ruschenplatt and Thomas (1980) estimated the time scale of the mixing for some massive binaries, in which effects of radiation pressure and degeneracy were considered:

$$\tau_{\text{diff}} \approx \frac{\bar{\mu}}{\Delta\mu} \frac{\delta^2(\nabla_{\text{ad}} - \nabla)}{12\phi(1-\beta)\nabla_{\text{ad}}} \frac{W^3}{H_p l c}, \quad (3)$$

here ∇_{ad} , ∇ and H_p have their usual meanings, $\bar{\mu}$ is the mean value of μ in the region of interest, W is its distance in depth, β is the ratio of gas pressure to total pressure, and $l = \frac{1}{\kappa\phi}$ and c are the mean free path and velocity of a photon, respectively. δ and ϕ are defined below :

$$\delta = -\left(\frac{\partial \ln \phi}{\partial \ln T}\right)_{P,\mu}, \phi = \left(\frac{\partial \ln \phi}{\partial \ln \mu}\right)_{P,T}. \quad (4)$$

A massive-main-sequence star ($15M_{\odot}$) with a helium envelope ($1M_{\odot}$) was examined in that paper. Roughly estimated from a discontinuous model, in which exists a jump from the region of lower mean molecular weight to a higher one, the star has $\tau_{\text{diff}} = 1.7 \times 10^4$ yrs if diffusion extends over the whole radiative envelope. Ulrich (1972) obtained a time scale of 400 yrs in a similar case. Thermohaline mixing was then treated as an instantaneous process for intermediate-mass and massive close binaries by some authors in previous studies (de Loore & Vanbeveren 1994; de Loore & Vanbeveren 1995). However the actual time is longer than 1.7×10^4 yrs for some reasons, e.g., $\Delta\mu$ decreases gradually while undergoing thermohaline mixing.

A binary $1.26M_{\odot} + 1.00M_{\odot}$ with an initial orbital period of 1.0 day is considered here to examine the effect of thermohaline mixing on low-mass binaries. In a low-mass binary, He-rich matter is usually accreted onto the surface of the secondary during the last phase of RLOF and the He-rich phenomenon is not very severe in the accreting matter. The hydrogen mass fraction of the accreting matter is therefore assumed to be $X = 0.5$ and helium mass fraction to be $Y = 0.48$, which is an extreme case for low-mass binaries since hydrogen abundance usually has not reached such a low value. Another remarkable feature for low-mass binaries is the existence of convective envelope, which may mix the accreting matter into the whole convective envelope very rapidly, minimizing thermohaline mixing in this region. We therefore show the profile of thermodynamical quantities ∇_{ad} and ∇ during RLOF in figure 1 to see the change of surface convective region caused by the increase of the mass. a, b and c represent the mass of the secondary at about 1.00,

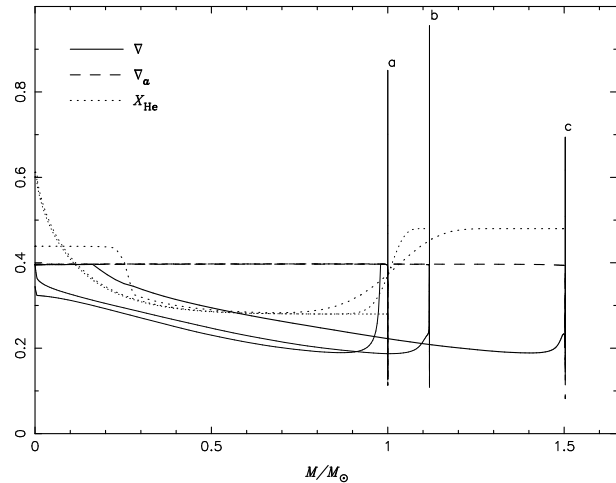


Figure 1. Profiles of adiabatic temperature gradient, real temperature gradient and helium composition at different masses that the accretor reaches. a, b and c represent the mass of 1.00 , 1.12 and $1.50 M_{\odot}$, respectively. Thermohaline mixing has not been included here.

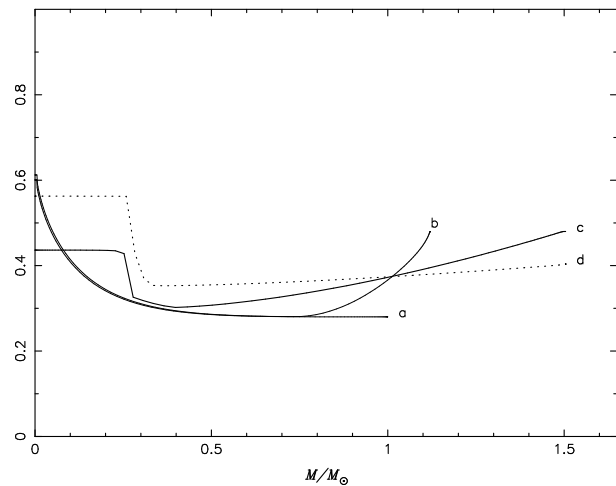


Figure 2. Helium profiles at different masses that the accretor reaches, themohaline mixing is added. a, b and c represent the mass of 1.00 , 1.12 and $1.50 M_{\odot}$, respectively. Dotted line represents the profile at an age of $\sim 5.3 \times 10^9$ yrs, 5×10^8 yrs older than that of line c, where the accretor just stops its accretion from the mass donor.

1.12 and $1.50 M_{\odot}$, respectively. The helium profile at corresponding masses is also shown in the figure. Thermohaline mixing has not been included in the figure yet.

We find in figure 1 that the surface convective region is very small and disappears quickly after a little matter is accreted, which cause He-rich matter pile up on the surface. In figure 1, the helium profiles are smoothed due to numerical diffusion owing to the moving non-Lagrangian mesh. A higher mesh resolution may improve it.

We stop the calculation when $0.5M_{\odot}$ matter is accreted. In Table 1, we show some thermodynamic quantities from the last model at the boundary of convective core, at which the mean molecular weight begins to increase outward (boundary of interest) and at the surface. We obtained $\tau_{\text{diff}} \approx 3.46 \times 10^8$ yrs from equation(3) and Table 1. It is more

Table 1. Data for a $1.5M_{\odot}$ star with a He-rich envelope. Radius, pressure scale height, photon mean free path, temperature gradient and the thermodynamic quantities $1 - \beta$, ∇_{ad} , δ^2/ϕ and $\bar{\mu}$ are given for different regions.

location	M_r/M_{\odot}	$r/10^{10}\text{cm}$	$H_p/10^8\text{cm}$	l/cm	∇	$1 - \beta$	∇_{ad}	δ^2/ϕ	$\bar{\mu}$
core	0.164	1.020	90.4	0.0177	0.396	0.0015	0.396	1.0061	1.529
boundary	0.692	2.000	64.0	0.0328	0.264	0.0011	0.397	1.0043	1.295
surface	1.503	8.303	1.8	2.7×10^7	0.125	0.0053	0.087	1.0213	1.607

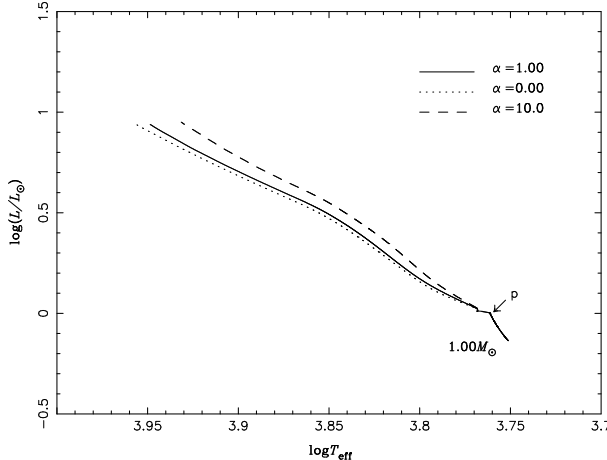


Figure 3. Evolutionary tracks of the secondaries during RLOF for models with and without thermohaline mixing.

than a quarter of the remaining main sequence time of the star after accretion ($\sim 1.35 \times 10^9$ yrs), which means that we can observe He-rich phenomenon for about at least a quarter of the life of the star left on the main sequence after accretion.

We now examine the effect via detailed calculations where thermohaline mixing is included as a diffusion process. The diffusion coefficient is defined as (see Kippehahn, Ruschenplatt & Thomas (1980))

$$D = \alpha \frac{H_p L^2}{(\nabla_{ad} - \nabla) \tau_{KH}} \left| \frac{d\mu}{dr} \right| \frac{1}{\mu} = \alpha \cdot 12 (1 - \beta) \frac{H_p l c \nabla_{ad} \phi}{(\nabla_{ad} - \nabla) \delta^2} \left| \frac{d\mu}{dr} \right| \frac{1}{\mu}, \quad (5)$$

where τ_{KH} and L can be considered as the Kelvin-Helmholtz time scale of perturbed blob and its radius, respectively. α is an efficiency parameter of order unity and can be increased to strengthen this mixing. The same model as above is calculated ($\alpha = 1.00$) and helium profiles at corresponding masses are shown in figure 2. The dotted line in the figure represents helium profile at an age of $\sim 5.3 \times 10^9$ yrs, where the star has evolved for some time after RLOF.

We find obvious differences in the helium profile between figure 1 and figure 2, which cause the final discrepancy of evolutionary tracks (figure 3). For comparison, the evolutionary track as $\alpha = 10.0$, which is very different from the case of $\alpha = 1.00$, is also presented in figure 3. The turn-off (point p) at the onset of RLOF in the figure results from a sudden change of surface composition. After RLOF, He-rich matter mixes inward quickly at first. However the mixing becomes slower and slower because of the decrease of $\Delta\mu$ and increase of W . The age at point c is about 4.8×10^9 yrs, 5×10^8 yrs younger than that of point d, however, we still see that μ slightly increases outwards in the envelope. It means

that the real time-scale of the mixing is much longer than the estimated value before.

For the reasons above, we prefer to a time-dependent way rather than an instantaneous process in treating thermohaline mixing in low-mass close binaries, especially when we are interested in the surface composition of the gainers. As convective time scale is much shorter than that of thermohaline mixing, we just consider the effect in radiative regions when we include thermohaline mixing.

4 RESULTS

As examples, we calculate a series of low-mass binaries to examine the effects of surface composition and thermohaline mixing on these objects. The initial mass of the primary M_1 has three values, 1.0, 1.26 and $1.6M_{\odot}$, in roughly equal intervals in $\log M_1$. The initial mass ratio $q_i = M_1/M_2$ of the systems is 1.1, 1.5 and 2.0. Case B evolution is simulated here and RLOF begins at early Hertzsprung-gap (Han et al. 2000; Chen & Han 2002; Chen & Han 2003). The models are calculated under four different assumptions: (a) the surface composition is assumed to remain unchanged during accretion; (b) chemical composition of the accreting matter is included via equation (2); (c) thermohaline mixing included based on (b), $\alpha = 1.00$; (d) similar to (c), but for $\alpha = 10^5$, which can be considered as an instantaneous assumption. Accretion rate and element abundances of the accreting matter are determined by the primaries.

Evolutionary tracks for models with the primary mass $1.26M_{\odot}$ are shown in figures 4, 5 and 6. We find obvious divergences of evolutionary loci in the three figures. The models under assumption (a) stay on the right and the ones with assumption (b) lie on the left. The dash-dotted lines, much closer to that of models (b) represent the ones with thermohaline mixing included ($\alpha = 1.0$) and the dashed lines are for $\alpha = 10^5$. From the three figures we see that, the change of surface composition, mainly the enhancement of helium abundance, makes the gainer hotter (or bluer), thermohaline mixing just slightly lessens the effect while the instantaneous mixing ($\alpha = 10^5$) may lessen the effect by much. All these finally cause corresponding divergences on CMD (figure 7).

At the onset of RLOF, surface convective regions exist in the secondaries, however, the accreting matter comes from the surface of the primaries and has a similar composition to that of the secondaries' surface, the evolutionary loci then show no differences in the three figures. When the composition of the accreting matter becomes quite different at the last phase of RLOF, surface convective regions of secondaries have already disappeared. Then some He-rich matter is piled up on the surface of the accretors. We see in

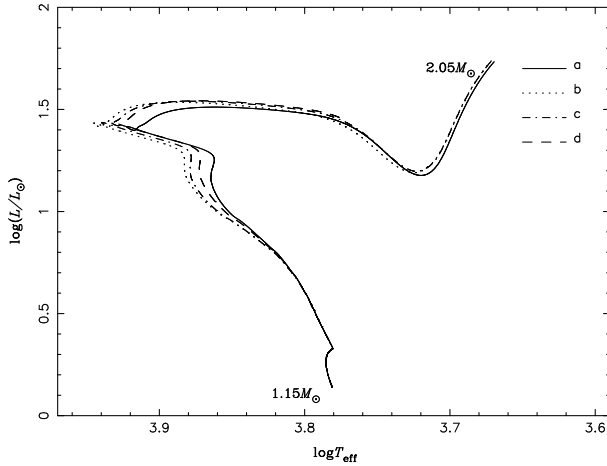


Figure 4. Evolutionary tracks of the secondary (evolving up from the bottom) under different assumptions for a binary of $1.26 + 1.15M_{\odot}$ ($q_i = 1.1$) with an initial orbital period of 0.943 days.

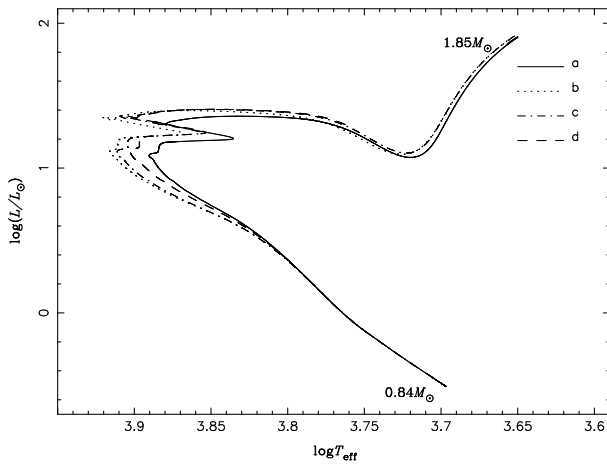


Figure 5. Similar to figure 4, but for a binary of $1.26 + 0.84M_{\odot}$ ($q_i = 1.5$) with an initial orbital period of 0.911 days.

figure 2 that thermohaline mixing has no effect on surface element abundances during RLOF, but it may redistribute the chemical composition in the interior (under the outermost layers) and affect the evolutionary tracks (figures 3 to 6).

We show some surface parameters of a binary with masses $1.26 + 0.63M_{\odot}$ and with an initial orbital period of 0.878 days in figure 8. The divergences of these parameters appear at the age $\log t(\text{yrs}) = 9.66$ when the surface hydrogen mass fraction has decreased obviously. In the figure we see that, with the decreasing of surface hydrogen, the star contracts slightly (which makes a increase of surface gravity) compared to the one with original surface composition. As well, the surface effective temperature has increased. The change of both temperature and radius (or gravity) leads to variations of colour indices of the star, which finally causes the change of position of the star on CMD (figure 7). Thermohaline mixing lessens the effect, but the lessening is slight during RLOF unless it were to act instantaneously, i.e. $\alpha = 10^5$. We also see that little distinction in surface hydrogen mass fraction X_H exists between the models with

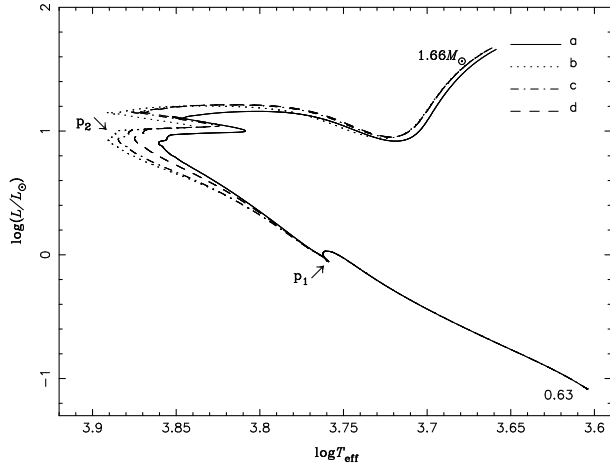


Figure 6. Similar to figure 4, but for a binary of $1.26 + 0.84M_{\odot}$ ($q_i = 2.0$) with an initial orbital period of 0.878 days.

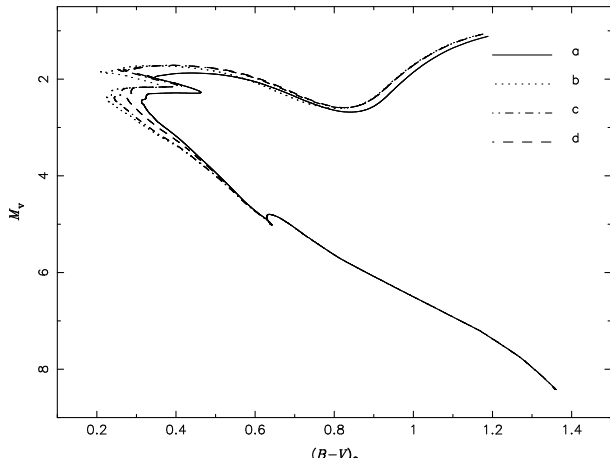


Figure 7. Evolutionary tracks of the secondary under different assumptions on color-magnitude diagram for a binary of $1.26 + 0.63M_{\odot}$ ($q_i = 2.0$) with an initial orbital period of 0.878 days.

and without thermohaline mixing before $\log t(\text{yrs}) = 9.79$ in figure 8. However there is a jump in X_H near the end of the main sequence, corresponding to the end of RLOF – no matter is accreted during this time, and thermohaline mixing makes surface hydrogen increase again.

There are two interesting turn-offs on the evolutionary tracks in figure 6. One is before the divergence of the loci (p_1) and the other is near the end of main sequence (p_2). The two points correspond to two abrupt changes of mass accretion rate during RLOF. The first is a sudden increase of mass accretion rate at the onset of RLOF, the mass increases from 0.63 to $1.1M_{\odot}$ in a very short time, and thermal adjustment of the star results in the first turn-off in the figure. The other turn-off is caused by the decrease of the mass accretion rate during the last phase of RLOF.

The variations of surface CNO abundances of the secondary for a binary $1.26 + 0.63M_{\odot}$ ($q_i = 2.0$) with an initial orbital period of 0.878 days under assumption (c) are shown in figure 9. It is not distinctly different from the one under assumption (b) except C increases and N decreases at $\log t(\text{yrs}) = 9.79$, which is caused by thermoha-

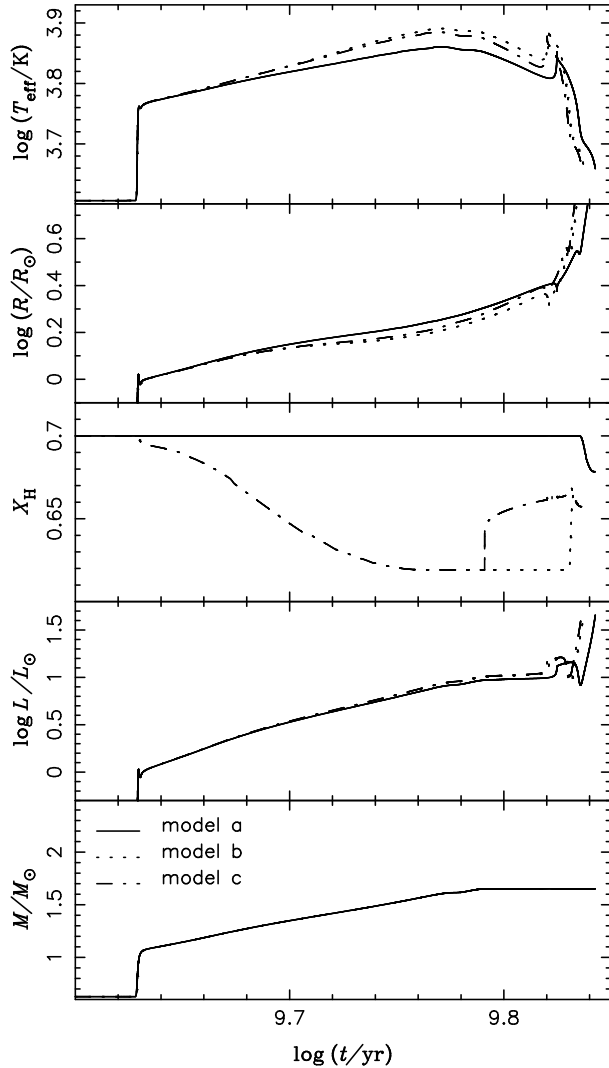


Figure 8. Some surface parameters change with age for a binary of $1.26 + 0.63M_{\odot}$ ($q_i = 2.0$) with an initial orbital period of 0.878 days.

line mixing taking effect on the surface abundances when accretion stops during this time. We find obvious changes of surface CNO abundances of the secondary during and after RLOF in the figure. The changes of N (increased) and C (decreased) begin at $\log t(\text{yrs}) = 9.63$ when the secondary mass is near $1.1M_{\odot}$. The surface convective region has already disappeared or will disappear soon for a star with this mass (see figure 1). With more matter lost from the primary, the change becomes more distinct – C is reduced from 0.0035 to 0.001 while N increases from 0.001 to 0.004 at $\log t(\text{yrs}) = 9.72$. Even after RLOF, CNO abundances also show obvious abnormalities – N is enhanced by nearly 150 per cent and C is decreased by nearly 50 per cent. It means that if a BS is formed by binary mass transfer, whether it is an Algol system or not, we should observe clear indication of some surface contamination by processed material spilled over from an evolved companion. CNO abundances of the accreting matter (from the primary) are also shown in the figure to check our code. The N discrepancy comes from the precision of $X + Y$, for N abundance is calculated

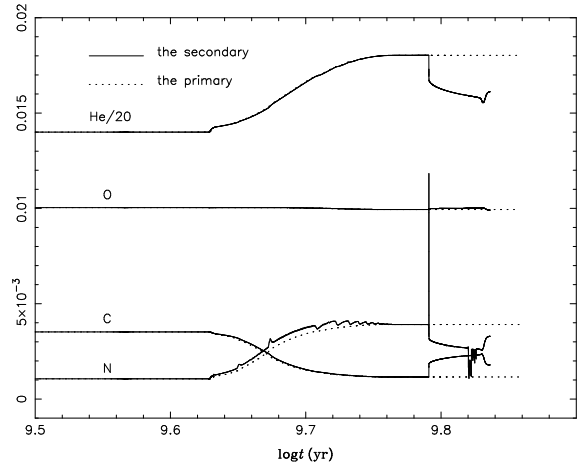


Figure 9. Helium and CNO surface abundances change with age for a binary of $1.26 + 0.63M_{\odot}$ ($q_i = 2.0$) with an initial orbital period of 0.878 days. Note the helium composition is divided by 20 in the figure.

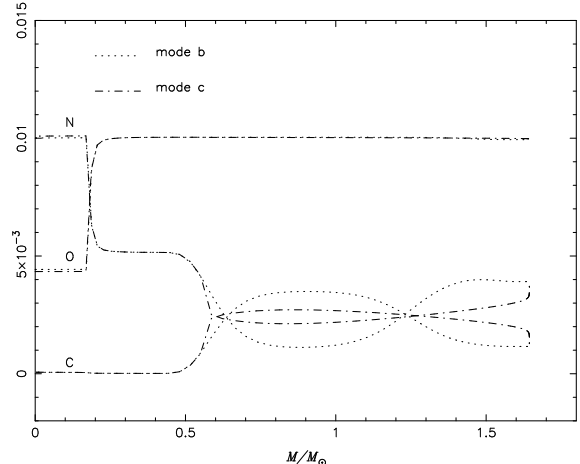


Figure 10. The profiles of CNO abundances of the accretor at the mass of about $1.64M_{\odot}$. The initial parameters of the system are $1.26 + 0.63M_{\odot}$ ($q_i = 2.0$) with an initial orbital period of 0.878 days.

by $X_N = 1.0 - X - Y - X_C - X_O - X_{Ne} - X_{Mg} - X_{Si} - X_{Fe}$ in our code. We cannot distinguish the models between assumption (b) and (c) via surface CNO abundances during RLOF as there is almost no difference in surface CNO composition between the models.

In order to examine the effect of thermohaline mixing, we show the profiles of CNO abundances in figure 10 when the secondary reaches $1.64M_{\odot}$. We see in the figure that the accreting matter has already mixed with the matter under the outer most envelope, as leads the change of overall stellar properties (figure 8).

The variations of chemical composition first result in the change of opacity, then other thermodynamic quantities, i.e. temperature, entropy, pressure etc.. Figure 11 shows the distribution of opacity for the accretor when it reaches $1.65M_{\odot}$ for the system above. In the figure, $\log \kappa$ of model (a) has already been distinguished from those of model (b) and (c), but the effect of thermohaline mixing is not very

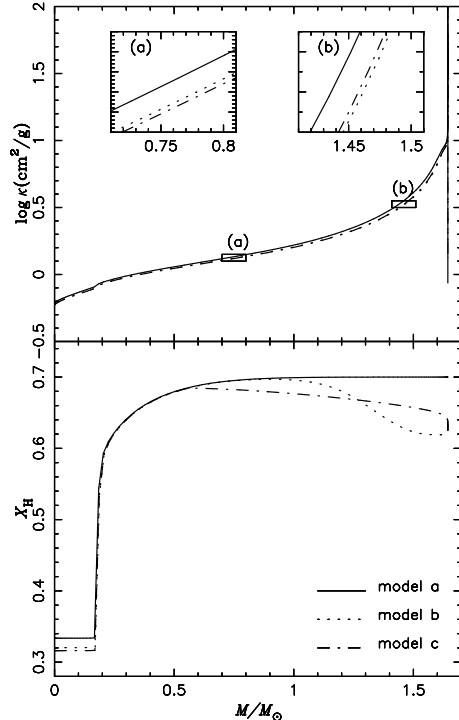


Figure 11. The profiles of opacity as the gainer reaches $1.64M_{\odot}$ for the binary $1.26 + 0.63M_{\odot}$ with $P_i = 0.878$ days.

remarkable – the difference on $\log \kappa$ between models (b) and (c) can only be seen by enlarging some parts of the figure. We may clearly see the influence of hydrogen mass fraction on opacity in the figure – larger hydrogen mass fraction results in larger opacity (it might be invalid at elsewhere as opacity also depends on temperature). The change of opacity mainly affects on the effective temperature, which can be seen in figure 8 – model (b) has a obviously higher surface effective temperature than model (a), while model(c) reduces this difference slightly.

As mentioned in section 1, a main-sequence accretor will go upwards along the main sequence in response to accretion and its main-sequence life will extend because hydrogen-rich matter mixes into the center. Here convective core is necessary to mix hydrogen-rich matter into the center. For a low-mass accretor without convective core at the onset of RLOF, central hydrogen does not increase until a convective core develops with mass increasing. After a convective core develops, further accretion will lead hydrogen-rich matter be involved in the convective core, increase the central hydrogen mass fraction and finally extend its life on the main sequence.

In Table 2, we summarize some system parameters when the secondaries leave the main sequence, i.e. the mass of the secondary, the orbital period and the age. We see that, when the secondaries leave the main sequence, many binaries are short-orbital-period systems, some of which are still in mass transfer. The distribution of periods is beyond our consideration here as it is related to initial orbital periods, but we may obtain a general ranges from previous grid calculations for low- and intermediate-mass binaries (Han et al. 2000; Chen & Han 2002; Chen & Han 2003). For low-mass binaries with their primary masses between $1-2M_{\odot}$, case B evolution

Table 2. System parameters when the secondaries leave off the main sequence. * represents that RLOF of the binary has not ceased yet at that time. The bottom part is for our simulation of F190. All the binaries are calculated under assumption (c).

M_{1i} (M_{\odot})	q_i	P_i (days)	M_2 (M_{\odot})	P (days)	t (yrs)	
1.00	1.1	0.590	1.3802	1.099	1.22E+10	*
1.00	1.5	0.545	1.4403	4.783	1.48E+10	
1.00	2.0	0.526	1.2845	3.152	1.72E+10	
1.26	1.1	0.943	1.9801	4.882	5.12E+09	*
1.26	1.5	0.911	1.8484	11.27	5.98E+09	
1.26	2.0	0.878	1.6508	7.412	6.62E+09	
1.60	1.1	1.511	2.701	27.65	2.29E+09	*
1.60	1.5	1.460	2.366	25.74	2.59E+09	
1.60	2.0	1.407	2.116	16.98	2.84E+09	
1.30	1.1	0.800	1.7710	1.43	4.45E+09	*
1.30	1.1	1.000	2.0480	4.95	4.49E+09	*
1.30	1.5	0.800	1.8739	11.00	5.55E+09	*
1.30	1.5	1.000	1.9238	13.09	5.20E+09	
1.30	2.0	0.800	1.6993	5.989	6.37E+09	*
1.30	2.0	1.000	1.7154	8.852	5.69E+09	
1.35	1.1	0.800	1.7809	1.272	3.87E+09	*
1.35	1.1	1.000	2.0794	4.070	3.96E+09	*
1.35	1.1	1.300	2.2287	12.46	3.97E+09	*
1.35	1.5	0.800	1.9263	5.908	4.91E+09	*
1.35	1.5	1.000	1.9981	14.01	4.64E+09	
1.35	2.0	0.800	1.7397	5.010	5.68E+09	*
1.35	2.0	1.000	1.7822	9.471	5.11E+09	
1.40	1.5	0.800	1.9840	5.492	4.39E+09	*
1.40	1.5	1.000	2.0750	15.01	4.14E+09	
1.40	2.0	0.800	1.7948	4.714	4.96E+09	*
1.40	2.0	1.000	1.8528	10.18	4.59E+09	
1.45	1.5	0.800	2.0413	5.048	4.00E+09	*
1.45	1.5	1.000	2.1548	16.09	3.70E+09	
1.45	1.5	1.300	2.1489	19.69	3.55E+09	
1.45	2.0	0.800	1.8458	4.290	4.72E+09	*
1.45	2.0	1.000	1.9245	10.91	4.11E+09	
1.45	2.0	1.300	1.9191	13.39	3.84E+09	
1.50	1.5	0.800	2.0630	3.753	3.68E+09	*
1.50	1.5	1.000	2.2350	16.82	3.29E+09	*
1.50	1.5	1.300	2.2315	21.12	3.16E+09	
1.50	2.0	0.800	1.8521	2.898	4.48E+09	*
1.50	2.0	1.000	1.9992	11.70	3.67E+09	
1.50	2.0	1.300	1.9938	14.36	3.41E+09	
1.55	1.5	0.800	2.0747	2.795	3.39E+09	*
1.55	1.5	1.000	2.3216	18.23	2.94E+09	*
1.55	1.5	1.300	2.3172	22.67	2.82E+09	
1.55	2.0	0.800	1.8428	1.979	4.23E+09	*
1.55	2.0	1.300	2.0704	15.41	3.08E+09	

does not result in long-orbital-period systems, and the periods are less than 40 days. It means that case B evolution may explain BSs phenomenon in binaries with orbital periods in this range, consistent with the results of Monte-Carlo simulations(Pols & Marinus 1994; Leonard 1996).

Table 3. Observational characters of F190. The third column gives the the references. 1-Gilliland et al.(1991), 2-Milone & Latham (1994), 3-Landsman et al.(1998), 4-Milone& Latham (1992).

<i>V</i>	10.92 - 10.95	1, 2, 3
<i>B</i> - <i>V</i>	0.22 - 0.25	1, 2, 3
<i>P</i>	4.18284 \pm 0.00015(d)	4
<i>e</i>	0.205 \pm 0.043	4
<i>f</i> (<i>M</i>)	0.0015 \pm 0.0002(<i>M</i> _○)	4
<i>T</i> _{eff}	7750(K) or 7610(K)	3
log <i>g</i>	3.78	3

Table 4. Observational characters of M67. *m* - *M* is the distance modulus. R represents references. 1, Carraro et al.(1996), 2-Janes & Smith (1984) and 3-Fan et al. (1996).

Age(Gyrs)	<i>m</i> - <i>M</i>	<i>E</i> (<i>B</i> - <i>V</i>)	[Fe/H]	R
4	9.65	0.025	-0.1	1
	9.48	0.056 \pm 0.006	-0.05 \pm 0.03	2
4	9.47 \pm 0.16	0.015-0.052	-0.10	3

5 F190

F190 is among the five bluest stragglers in old open cluster M67. It has been suspected of being a spectroscopic binary with an orbital period of about 4 days. An orbital solution of the star and its elements were published in 1992 (Milone & Latham 1992) in which the period was confirmed to be about 4.18 days. Tables 3 and 4 list some observations in recent years for F190 and M67, respectively.

Milone & Latham (1992) estimated the mass of the primary (the BS) to be in the range of 2.0 to $2.2M_{\odot}$ based on two extreme assumptions on evolutionary position and amount of light contributed by the secondary. If we suppose that mass transfer began fairly recently, and that the turnoff mass (of M67) was only slightly larger than $1.26M_{\odot}$ - the turnoff mass according to Vandenberg(1985), then the initial mass of the binary could not exceed about $2.5M_{\odot}$, which means that mass transfer has been quite efficient and very little mass was lost from the system (Milone & Latham 1992). In this section, we simulate mass transfer history of this object based on assumption(c) as above.

Following constraints are considered when we define the ranges of our data cube:

- the mass of the primary should be larger than the turnoff mass of M67. Meanwhile, previous calculations (Han et al. 2000; Chen & Han 2002; Chen & Han 2003) show that a mass of $1.6M_{\odot}$ for the primary is too large, the orbital period of a binary with primary mass of $1.6M_{\odot}$ is always larger than 4 days at a age longer than 3 Gyrs via case B evolution. The primary mass then ranges from 1.30 to $1.55M_{\odot}$ at intervals of $0.05M_{\odot}$. We will see later that, even for case A evolution, $1.6M_{\odot}$ is an appropriate upper limit of the primary for F190.

- the mass ratio of the systems should not be very large in order to avoid the formation of a common envelope. The chosen initial mass ratio is 1.1, 1.5 and 2.0 in our calculations.

- the initial orbital period is 0.8, 1.0 and 1.3 days for each system to ensure the onset of RLOF during HG or near to HG (at the end of main sequence).

Characteristics for all of the binaries during RLOF are listed in Table A1. Some parameters of the secondaries are shown in Table 5 when the orbital period is about 4.2 days. Visual magnitude in V band *M*_v is calculated by

$$M_v = M_{\text{bol}} - BC, \quad M_{\text{bol}} = 4.75 - 2.5 \times \log(L/L_{\odot}), \quad (6)$$

BC, *B* - *V* and *U* - *B* are obtained by linear interpolation from BaSel-2.0 model (Lejeune, Cuisinier & Busel 1997; Lejeune, Cuisinier & Busel 1998) via temperature *T* and log*g*. Although the metallicity of M67 is a little different from solar (Table 4), the difference is small. Meanwhile some other studies concur that the metallicity of M67 is virtually indistinguishable from solar, i.e. [Fe/H] = -0.09 ± 0.07 according to Friel & Janes(1993), [Fe/H] = -0.04 ± 0.12 according to Hobbs & Thorburn (1991). Therefore we choose the table of [Fe/H] = 0.0 when we interpolate, consistent with the model calculations.

In Table 5, we see that the surface abundances of He, C, N, O are obviously abnormal (the normal values are 0.28000, 0.00352, 0.00106 and 0.01004, respectively). Meanwhile, all the models are in slow mass transfer with a rate $\sim 10^{-10}M_{\odot}\text{yr}^{-1}$, which is consistent to the argument of Milone & Latham (1992) that a final slow stage of mass transfer is still underway for the F190. We also see that, when (*P*_i, *q*_i) is constant, the gainer is younger at the period of 4.2 days with the increase of primary's mass until the system becomes a contact binary finally. As *M*_{1i} > $1.5M_{\odot}$, the system is either contact or younger than 3 Gyrs when the orbital period is about 4.2 days. The value of $1.6M_{\odot}$ is therefore a 'safe' upper limit of the primary mass as we study the mass-transfer history of F190, including case A evolution.

To find out the appropriate models for F190, we show the location of F190 in the model grid in figure 12 with some constraints included, i.e. the system's orbital period (3.2 - 5.2 days) and the age of the models (3 - 5×10^9 yrs) are around 4.2 days and 4 Gyrs, respectively. The flexible ranges of orbital period and age are chosen here as there are errors between theory models and observations, e.g., due to the coarseness of the grid the models cannot be expected to fit the observations exactly. The position range of F190 by observations is also shown in the figure. The distance modulus *m* - *M* of M67 ranges from 9.45 to 9.65 while *V* = 10.95, *B* - *V* ranges from 0.22 to 0.25. Three evolutionary tracks under these constraints pass through the area of F190 in the figure. The initial parameters for the three models are (*M*_{1i}, *q*_i, *P*_i) = (1.40, 1.5, 0.8), (1.40, 2.0, 0.8), (1.45, 1.5, 0.8) from the bottom right to the top left in the area of F190, respectively. However, the secondary in the model with (*M*_{1i}, *q*_i, *P*_i) = (1.40, 2.0, 0.8) has already left the main sequence and cannot be considered as a BS. The primary's mass of appropriate models for F190 is then located in the range of 1.40 to $1.45M_{\odot}$ with (*q*_i, *P*_i) = (1.5, 0.8). The best-fitting model is a binary with (*M*_{1i}, *q*_i, *P*_i) = (1.45, 1.5, 0.8). Parameters of the system at the orbital period about of 4.2 days are *M*₂ = $2.0M_{\odot}$, *M*_v = 1.316, *B* - *V* = 0.222 and the age *t* = 3.95×10^9 yrs, which fit the observations well.

Figures 13 and 14 show the evolutionary tracks of binaries (*M*_{1i}, *q*_i, *P*_i) = (1.40, 1.5, 0.8) and (1.45, 1.5, 0.8), respec-

Table 5. Parameters of the secondaries at orbital period of about 4.2 days.

M_{1i} (M_{\odot})	P_i (days)	q_i	M_2 (M_{\odot})	X_H^c	t (10^9 yrs)	M_v	$B - V$	$U - B$	X_{He}^s	X_{C}^s	X_{N}^s	X_{O}^s	\dot{M} ($M_{\odot} \text{ yr}^{-1}$)
1.30	0.80	1.1	contact										
	1.00	1.1	2.016	0.046	4.45	1.317	0.204	0.125	0.335	0.00176	0.00316	0.00989	8.790E-10
	0.80	1.5	1.814	0.191	5.35	1.800	0.252	0.098	0.343	0.00142	0.00342	0.00996	4.551E-10
	1.00	1.5	1.779	0.480	4.60	2.026	0.125	0.085	0.343	0.00151	0.00341	0.00988	6.084E-10
	0.80	2.0	1.661	0.166	6.16	2.178	0.338	0.017	0.353	0.00108	0.00376	0.00996	2.568E-10
	1.00	2.0	1.632	0.517	4.76	2.394	0.192	0.075	0.357	0.00116	0.00378	0.00987	3.758E-10
1.35	0.80	1.1	contact										
	1.00	1.1	2.086	0.000	3.97	0.936	0.057	0.091	0.331	0.00175	0.00307	0.00995	9.229E-10
	1.30	1.1	2.025	0.288	3.76	1.388	0.088	0.102	0.326	0.00192	0.00289	0.00995	1.421E-09
	0.80	1.5	1.878	0.122	4.80	1.636	0.261	0.106	0.340	0.00138	0.00342	0.00998	4.694E-10
	1.00	1.5	1.842	0.449	4.14	1.871	0.109	0.088	0.339	0.00149	0.00336	0.00993	6.175E-10
	0.80	2.0	1.719	0.073	5.59	2.022	0.355	0.010	0.349	0.00105	0.00376	0.00997	2.810E-10
1.40	1.00	2.0	1.690	0.473	4.36	2.225	0.175	0.082	0.352	0.00113	0.00377	0.00988	3.872E-10
	0.80	1.5	1.944	0.101	4.31	1.469	0.247	0.115	0.338	0.00129	0.00355	0.00992	5.065E-10
	1.00	1.5	1.906	0.418	3.73	1.719	0.092	0.088	0.336	0.00142	0.00348	0.00986	6.571E-10
	0.80	2.0	1.781	0.042	4.92	1.843	0.329	0.034	0.346	0.00096	0.00389	0.00992	3.037E-10
1.45	1.00	2.0	1.750	0.451	3.98	2.057	0.152	0.089	0.348	0.00107	0.00386	0.00983	4.166E-10
	0.80	1.5	2.012	0.073	3.95	1.316	0.222	0.124	0.339	0.00122	0.00364	0.00989	5.684E-10
	1.00	1.5	1.973	0.400	3.34	1.581	0.075	0.080	0.335	0.00139	0.00346	0.00989	7.164E-10
	1.30	1.5	1.920	0.572	2.95	1.850	0.048	0.041	0.334	0.00154	0.00337	0.00984	1.174E-09
	0.80	2.0	1.843	0.001	4.71	1.413	0.151	0.130	0.349	0.00087	0.00403	0.00985	3.434E-10
	1.00	2.0	1.812	0.427	3.61	1.909	0.129	0.092	0.346	0.00104	0.00388	0.00983	4.438E-10
1.50	1.30	2.0	1.770	0.621	2.96	2.190	0.096	0.069	0.348	0.00115	0.00385	0.00976	7.801E-10
	0.80	1.5	2.083	0.000	3.71	0.794	0.123	0.794	0.339	0.00114	0.00376	0.00983	6.135E-10
	1.00	1.5	2.042	0.389	2.98	1.452	0.055	0.065	0.334	0.00133	0.00385	0.00984	7.928E-10
	1.30	1.5	1.987	0.564	2.62	1.730	0.029	0.019	0.333	0.00148	0.00347	0.00980	1.318E-09
	0.80	2.0	1.908	0.000	4.62	1.691	0.978	0.712	0.307	0.00204	0.00629	0.00996	3.959E-10
	1.00	2.0	1.876	0.409	3.24	1.768	0.107	0.092	0.345	0.00098	0.00398	0.00977	4.933E-10
1.55	1.30	2.0	1.832	0.615	2.64	2.055	0.071	0.058	0.346	0.00110	0.00395	0.00970	8.653E-10
	0.80	1.5	2.114	0.415	2.63	1.362	0.025	0.028	0.336	0.00123	0.00376	0.00974	9.226E-10
	1.00	1.5	2.057	0.573	2.34	1.613	0.010	-0.002	0.334	0.00142	0.00366	0.00973	1.486E-09
	0.80	2.0	contact										
	1.00	2.0	contact										
	1.30	2.0	1.896	0.611	2.37	1.938	0.047	0.036	0.348	0.00104	0.00412	0.00961	9.924E-10

tively. The locations of both components as the secondaries is in the observational region of F190 are ranged out by pluses in the two figures. We see that the surface effective temperature of the secondaries is in $3.88 < \log T_{\text{eff}} < 3.89$ if M_2 is located in the observational region of F190, very close to the value given by Landsman et al. (1998) ($\log T_{\text{eff}} = 3.889$ and 3.881 for $T_{\text{eff}} = 7750$ K and 7610 K, respectively). However, the surface gravity in the two models ($\log g$ in the region 3.87-3.91) is a little bigger than the value given in Table 3. Both the two systems begin RLOF near the end of the main sequence (see also Table A1), indicating that case A is a more likely channel to form F190, different from what has long been suspected that case B mass transfer leads the formation of the object (Milone & Latham 1992; Leonard 1996). The property of the companion (M_1) is worth a mention. In figure 13, $M_v = 3.65$ and 3.41 for M_1 as its mass equal to 0.40 and $0.36 M_{\odot}$, respectively. In figure 14, M_v of the primary is about 3.55 as the secondary in the obser-

vational area of F190. This result means that it is hard to detect the signal from the companion by spectroscopic except for a very high ratio of signal to noise (e.g. $S/N \geq 500$). Meanwhile, IUE spectra (Landsman et al. 1998) show no evidence for a hot subluminous companion for F190, indicating that the companion is likely a cool star, which is consistent with the position shown in the figures 13 and 14.

Orbital solutions of F190 (Milone & Latham 1992) showed that the object is an eccentric binary. Mass transfer cannot explain the phenomenon since tidal effects should have circularized the orbit of a binary with such a short orbital period. Milone & Latham (1992) mentioned that the eccentric orbit might be an artifact caused by some sort of line asymmetries in orbital solutions, or a resonant phenomena in an accretion disk, or a consequence of modulation by a distant third star in a wide orbit. Hurley et al. (2001) obtained two BSs in short-period eccentric orbits via a collision within a triple system, and suggested that F190 might

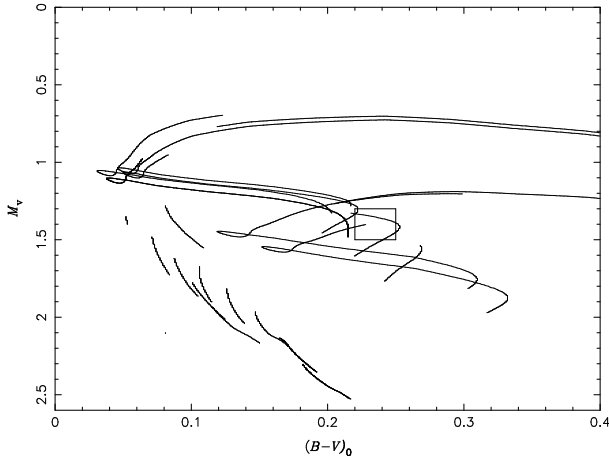


Figure 12. Evolutionary tracks of the secondaries on color-magnitude diagram when the system's orbital period is between 3.2 days and 5.2 days and the age changes from 3×10^9 to 5×10^9 yrs. Observational range of F190 is determined by a distance modulus $m - M = 9.45 - 9.65$ with $V = 10.95$, $B - V = 0.22 - 0.25$. Three lines go across the range of F190. Parameters for the three lines (from the bottom right to the top left) are $(M_{1i}, q_i, P_i) = (1.40, 1.5, 0.8), (1.40, 2.0, 0.8), (1.45, 1.5, 0.80)$, respectively.

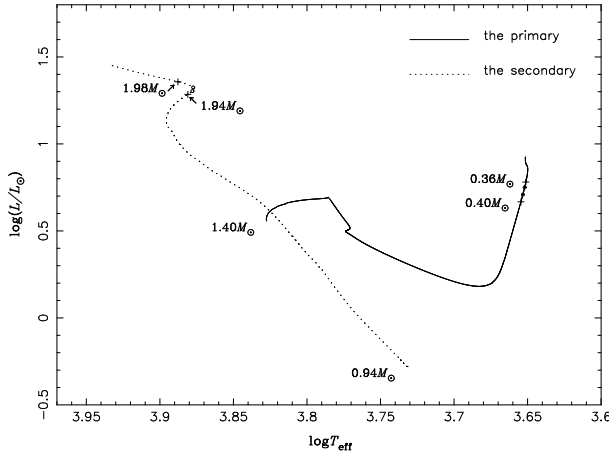


Figure 13. Evolutionary tracks of both components for a binary $1.40 + 0.93 M_\odot$ with an initial orbital period 0.80 days. The part between two pluses, except the part between two circles, represent the secondary stays in the region of F190 by observation.

be produced in this way. Sandquist et al. (2003) reported that BS S1082 in M67 is a possible triple (see also van den Berg et al. (2001)). Meanwhile, orbital evolution in triples shows that a third star may indeed induce eccentricity in the orbit of a close binary (Eggleton & Kiseleva-Eggleton 2001). If the eccentricity is real and induced by a triple companion or an encounter with a third body, then the orbital period is modified after RLOF. In this case the current orbital parameters do not result purely from RLOF, and our procedure of fitting the period will not give the correct initial parameters.

6 DISCUSSIONS AND CONCLUSIONS

In the investigation, we studied the structure and evolution of the mass gainers on the main sequence for low-mass bi-

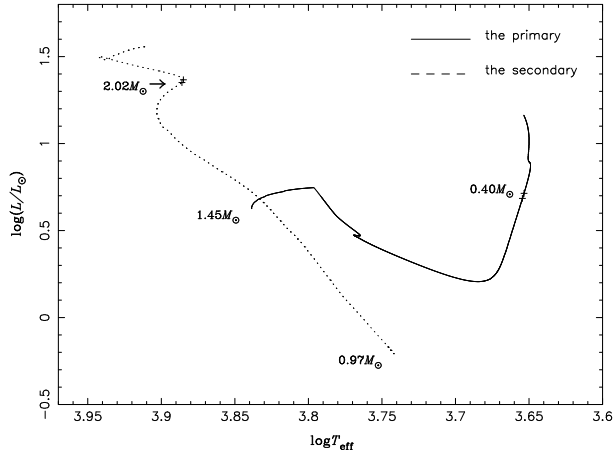


Figure 14. Evolutionary tracks of both components for a binary $1.45 + 0.97 M_\odot$ with an initial orbital period 0.80 days. The part between two pluses represent the secondary stays in the region of F190 by observation.

naries under different assumptions (see section 4). We see that the decrease of hydrogen mass fraction on the surface (assumption (b)) makes the gainer bluer and smaller than the ones with original surface composition (assumption (a)) while thermohaline mixing (assumption (c)) lessens the effect slightly. If thermohaline mixing were to act instantaneously (assumption (d)), the effect would be lessened more. However the effect is small and probably cannot be observed. Meanwhile, thermohaline mixing (either instantaneous or not) causes composition redistribution in the envelopes, but not in the outer most regions during RLOF because of continuous accretion. Therefore obvious CNO abundance abnormalities, originating from matter that was originally in the inner regions of the primary, exist on the surfaces of the secondary during RLOF under assumptions (b), (c) and (d). After RLOF, CNO abundance abnormalities are greatly weakened under assumptions (c) and (d) by thermohaline mixing taking effect on the surface abundances, but element contamination (from the primary) will not disappear. We therefore prefer to a time-dependent way rather than an instantaneous process in treating thermohaline mixing when we study the BSs formed by mass transfer.

Some secondaries are still near the end of RLOF at the age larger than that of M67 in our simulations. The orbital period after RLOF in our calculations and previous results for low-mass binaries ranges from several days to tens of days. It means that case A and case B mass transfer may produce BSs in short- or relatively short-orbital-periods binaries (including Algol systems), i.e. the orbital period less than forty days. This result consistent with the Monte-Carlo simulation by some authors (Pols & Marinus 1994; Leonard & Peter 1996). Further constraints to the range of orbital period of BSs formed via this channel need binary population synthesis.

As we simulate BSs formed via binary mass transfer, some physical constraints should be considered to limit initial models. At first, the system should avoid common envelope – a more complex case and we will study it in the future. It means that the initial mass ratio should not be very large and the primary has a radiative envelope when RLOF starts.

Secondly, the primary cannot be much more massive than the turn-off mass of the cluster, or it evolves very fast, the secondary then increases to a high mass in a very short time and evolves rapidly after a short self-adjustment. As a consequence, the secondary should have left the main sequence at the age of the host cluster, then cannot be recognized as a BS. Combining these considerations with observations of F190 and M67, we ranged the initial parameters of the object F190 by complete grid simulations. We find that the primary's mass in appropriate models for F190 is located in the range of 1.40 to $1.45M_{\odot}$ with $(q_i, P_i) = (1.5, 0.8)$ and that case A evolution is a more likely evolutionary channel than case B to form this object. Evolutionary locations of both components for two appropriate models are presented in the paper to help determine the companion of F190. Our simulation indicates that F190 is still in slow mass transfer phase and exists obvious CNO abundance abnormalities. The abnormalities might be observed later.

As there are very few BSs in short-orbital-period systems observationally, binary merger (case A) and case C mass transfer may be the main sources of BSs among binary interactions. However binary merger is a very complex process during which much physics is not very clear yet. An initial model of a merger can just be constructed based on relatively clear physical phases and some assumptions, i.e. the degree of matter mixing. For case C mass transfer, finding out the region of initial mass ratio to avoid dynamical instability is important. We will study both of the two cases in our following work.

ACKNOWLEDGMENTS

We thank Prof. B. Shustov for his kind help. We also thank Prof. S. M. Andervisky, Dr. Ph. Podsiadlowski, Dr. F. Zhang and Sh. Gu for their helpful suggestions and discussions on the subject. We are grateful to the referee for his useful and inspirational suggestions which help us improve the paper greatly. This work is supported by the Chinese National Science Foundation (Grant No. 19925312), the Chinese Academy of Sciences (No. KJCX2-SW-T06), and the 973 Scheme (NKBRSF No. G19990754).

REFERENCES

Alexander D.R., Ferguson J.W., 1994a, in Jorgensen U.G., ed., Molecules in the stellar Environment. Springer-Verlag, Berlin, p.149

Alexander D.R., Ferguson J.W., 1994b, ApJ, 437, 879

Carney,B.W., Latham,D.W., Laird,J.B., Grant,C.E., Morse,J.A., 2001, AAS, 199,0706

Carraro, G., Girardi, L., Bressan, A. & Chiosi, C., 1996, A&A, 305, 849

Chen Xuefei, Han Zhanwen, 2002, MNRAS, 335, 948

Chen X., Han Z., 2003, MNRAS, 341, 662

Collier, A., Jenkins, C., 1984, MNRAS, 211, 391

de Loore, C., Vanbevern, D., 1994, A&A, 292, 463

de Loore, C., Vanbevern, D., 1995, A&A, 304, 220

Deng L., Chen R., Liu X., Chen J., 1999, ApJ, 524, 824

Eggleton P.P., 1971, MNRAS, 151, 351

Eggleton P.P., 1972, MNRAS, 156, 361

Eggleton P.P., 1973, MNRAS, 163, 179

Eggleton P.P., Kiseleva-Eggleton L., 2001, ApJ, 562, 1021

Fan, X., et al. 1996, AJ, 112, 628

Friel, E., D., Janes,k., A., 1993, A&A, 267, 75

Gilliland, R.L., Brown,T.M., Duncan,D.K.,Suntzeff,N.B., Lockwood, G.W., Thompson, D.T., Schild, R.E., Jeffrey, W.A., & Penprase, B.E., 1991, AJ, 101, 541

Han Z., Podsiadlowski Ph., Eggleton P.P., 1994, MNRAS, 270, 121

Han Z., Tout C.A., Eggleton P.P., 2000, MNRAS, 319, 215

Hellings, P., 1984, ApSS, 104, 83

Hobbs, L.M., Thorburn, J.A., 1991, AJ, 102, 1070

Hurley, J., Tout, C. A., Aarseth S. J., Pols, O. R., 2001, MNRAS, 323, 630

Hurley, J., Tout, C. A., Pols, O. R., 2002, MNRAS, 329, 897

Iglesias C. A., Rogers F. J., 1996, ApJ, 464, 943

Janes, K.A. & Smith, G.H., 1984, AJ, 89, 487

Kippenhanhn, R., Ruschenplatt, G., Thomas, H.-C., 1980, A&A, 91, 175

Landsam, W., Bohl, R.C., Neff, S.G., O'Commell, R.W., Roberts, M.S., 1998, AJ, 116, 789

Lejeune, T., Cuisinier, F., Busel, R., 1997, A&AS, 125, 229

Lejeune, T., Cuisinier, F., Busel, R., 1998, A&AS, 130, 65

Leonard P. J. T., 1996, ApJ, 470, 521

Leonard,P. J. T., Peter J. T., 1996, ApJ, 470, 521

Marks, P. B., Sarna, M. J., 1998, MNRAS, 301, 699

McCrea, W. H., 1964, MNRAS, 128, 147

Milone, A. A. E., Latham, D. W., 1992, in Kondo Y., Sistero R. F., Polidan R. S., eds, Proc. IAU Symp. 151, Evolutionary Processes in Interacting Binary Stars, Vol.7. Kluwer, Dordrecht, P.475-478

Milone, A. A. E., Latham, D. W., 1994, AJ, 108, 1828

Nelson, C. A., Eggleton, P. P., 2001, ApJ, 552, 664

Peterson, R. C., Carney, B. W., Latham, D. W., 1984, ApJ, 279, 237

Pols O. R., Marinus M., 1994, A&A, 288, 475

Pols O.R., Schröder K.-P., Hurley J.R., Tout C.A., Eggleton P.P., 1998, MNRAS, 298, 525

Pols O.R., Tout C.A., Eggleton P.P., Han Z., 1995, MNRAS, 274, 964

Sandquist E. L., Latham D. W., Shetrone M. D., Milone A.A.E., 2003, AJ, 125, 810

Stryker, L.L., 1993, PASP, 105, 1081

Ulrich, R.K., 1972, ApJ, 172, 165

van der Berg, M., Orosz, J., Verbunt, F., Stassum, K., 2001, A&A, 375, 375

VandenBerg, D. A., 1985, ApJS, 58, 711

van den Heuvel, E. H. J., 1994, in 'Interacting Binaries', Saas-Fee Advanced Course 22, eds. H. Nussbaumer and A. Orr, Springer Verlag, Berlin

Wellstein S., Langer N., Braun H., 2001, A&A, 369, 939

APPENDIX A: RLOF FOR ALL THE BINARIES

Table A1 lists all the binaries simulating F190 in Sect.5:

a: the onset of RLOF

b: the minimum luminosity during RLOF (i.e., just reaching the RGB)

c: at the end of RLOF (RLOF may have several episodes, there is no RLOF any more after c)

d: at the end of calculation

We usually list stellar parameters at a, b, c and d. However, the code breaks down when RLOF is unstable. In that case, we only list parameters at a if RLOF is unstable at onset, or at a and b if RLOF is stable at the onset but becomes unstable after primary reaching RGB.

Table A1. RLOF of all the binaries simulated for a BS of F190.

	t_1 (yr)	M_1 (M_\odot)	\dot{M}_1 ($M_\odot \text{yr}^{-1}$)	X_H^c	X_H^s	q	M_2 (M_\odot)	P (days)
a	3.334×10^9	1.303	0.000	0.000	0.700	1.096	1.189	0.8000
b	4.268×10^9	0.866	-8.626×10^{-10}	0.000	0.688	0.533	1.625	1.064
c	5.224×10^9	0.256	-3.507×10^{-12}	0.000	0.644	0.115	2.236	15.84
d	5.253×10^9	0.256	0.000	0.000	0.644	0.115	2.236	15.84
a	3.717×10^9	1.303	0.000	0.000	0.700	1.096	1.189	1.000
b	4.071×10^9	0.920	-2.161×10^{-9}	0.000	0.687	0.585	1.572	1.229
c	4.770×10^9	0.261	-1.113×10^{-12}	0.000	0.646	0.117	2.231	18.79
d	4.795×10^9	0.261	0.000	0.000	0.646	0.117	2.231	18.79
a	4.034×10^9	1.303	0.000	0.000	0.699	1.096	1.189	1.300
b	4.039×10^9	1.251	-5.337×10^{-10}	0.000	0.699	1.009	1.240	1.292
a	3.356×10^9	1.303	0.000	0.000	0.700	1.496	0.871	0.8000
b	4.428×10^9	0.761	-5.598×10^{-10}	0.000	0.682	0.539	1.413	0.9406
c	5.700×10^9	0.246	-2.413×10^{-12}	0.000	0.637	0.127	1.928	11.00
d	5.754×10^9	0.246	0.000	0.000	0.637	0.127	1.928	11.00
a	3.768×10^9	1.303	0.000	0.000	0.700	1.496	0.871	1.000
b	4.050×10^9	0.817	-1.514×10^{-9}	0.000	0.684	0.602	1.357	1.073
c	4.939×10^9	0.250	-1.120×10^{-12}	0.000	0.637	0.130	1.924	13.09
d	4.976×10^9	0.250	0.000	0.000	0.637	0.130	1.924	13.09
a	4.048×10^9	1.303	0.000	0.000	0.699	1.496	0.871	1.300
a	3.435×10^9	1.303	0.000	0.000	0.700	2.000	0.652	0.8000
b	4.607×10^9	0.667	-2.547×10^{-10}	0.000	0.678	0.518	1.288	0.7734
c	6.488×10^9	0.235	0.000	0.000	0.627	0.137	1.720	7.410
d	2.859×10^{10}	0.235	0.000	0.000	0.627	0.137	1.720	7.410
a	3.814×10^9	1.303	0.000	0.000	0.700	2.000	0.652	1.000
b	3.982×10^9	0.700	-9.078×10^{-10}	0.000	0.678	0.558	1.255	0.9034
c	5.107×10^9	0.239	-1.569×10^{-12}	0.000	0.623	0.139	1.715	8.852
d	2.636×10^{10}	0.239	0.000	0.000	0.623	0.139	1.715	8.852
a	4.065×10^9	1.303	0.000	0.000	0.698	2.000	0.652	1.300
a	2.959×10^9	1.349	0.000	0.017	0.700	1.097	1.230	0.8000
b	3.776×10^9	0.883	-9.677×10^{-10}	0.000	0.688	0.520	1.696	1.089
c	4.708×10^9	0.258	0.000	0.000	0.647	0.111	2.321	16.97
d	4.735×10^9	0.258	0.000	0.000	0.647	0.111	2.321	16.97
a	3.193×10^9	1.349	0.000	0.000	0.700	1.097	1.230	1.000
b	3.597×10^9	0.940	-2.156×10^{-9}	0.000	0.687	0.574	1.639	1.249
c	4.284×10^9	0.263	-3.791×10^{-12}	0.000	0.649	0.114	2.316	20.13
d	4.308×10^9	0.263	0.000	0.000	0.649	0.114	2.316	20.13
a	3.531×10^9	1.349	0.000	0.000	0.700	1.097	1.230	1.300
b	3.568×10^9	1.009	-6.358×10^{-9}	0.000	0.686	0.642	1.571	1.495
c	4.045×10^9	0.270	-6.628×10^{-12}	0.000	0.653	0.117	2.310	24.61
d	4.066×10^9	0.270	0.000	0.000	0.653	0.117	2.310	24.61
a	2.989×10^9	1.349	0.000	0.003	0.700	1.496	0.902	0.8000
b	3.897×10^9	0.785	-5.940×10^{-10}	0.000	0.684	0.535	1.466	0.9457
c	5.148×10^9	0.248	-1.002×10^{-12}	0.000	0.640	0.124	2.003	11.78
d	5.190×10^9	0.248	0.000	0.000	0.640	0.124	2.003	11.78
a	3.238×10^9	1.349	0.000	0.000	0.700	1.496	0.902	1.000
b	3.596×10^9	0.826	-1.424×10^{-9}	0.000	0.683	0.580	1.424	1.103
c	4.480×10^9	0.252	-3.474×10^{-12}	0.000	0.641	0.126	1.998	14.01
d	4.514×10^9	0.252	0.000	0.000	0.641	0.126	1.998	14.01

continued to next paper

Table A1. -continued

	t_1 (yr)	M_1 (M_\odot)	\dot{M}_1 ($M_\odot \text{yr}^{-1}$)	X_H^c	X_H^s	q	M_2 (M_\odot)	P (days)
a	3.547×10^9	1.349	0.000	0.000	0.699	1.496	0.902	1.300
a	2.994×10^9	1.349	0.000	0.000	0.700	2.000	0.675	0.8000
b	4.113×10^9	0.680	-2.742×10^{-10}	0.000	0.678	0.506	1.343	0.7901
c	5.933×10^9	0.237	-1.151×10^{-12}	0.000	0.631	0.133	1.786	7.934
d	2.782×10^{10}	0.237	0.000	0.000	0.631	0.133	1.786	7.934
a	3.285×10^9	1.349	0.000	0.000	0.700	2.000	0.675	1.000
b	3.534×10^9	0.721	-7.896×10^{-10}	0.000	0.678	0.553	1.303	0.9099
c	4.709×10^9	0.241	-1.727×10^{-12}	0.000	0.628	0.135	1.782	9.471
d	2.583×10^{10}	0.241	0.000	0.000	0.628	0.135	1.782	9.471
a	3.563×10^9	1.349	0.000	0.000	0.699	2.000	0.675	1.300
a	2.551×10^9	1.396	0.000	0.060	0.700	1.496	0.933	0.8000
b	3.485×10^9	0.795	-6.560×10^{-10}	0.000	0.684	0.518	1.534	0.9743
c	4.656×10^9	0.250	-5.982×10^{-12}	0.000	0.642	0.120	2.080	12.63
d	4.694×10^9	0.250	0.000	0.000	0.642	0.120	2.080	12.63
a	2.789×10^9	1.396	0.000	0.000	0.700	1.496	0.933	1.000
b	3.198×10^9	0.851	-1.453×10^{-9}	0.000	0.684	0.575	1.479	1.111
c	4.066×10^9	0.255	-4.557×10^{-12}	0.000	0.644	0.123	2.075	15.01
d	4.097×10^9	0.255	0.000	0.000	0.644	0.123	2.075	15.01
a	3.103×10^9	1.396	0.000	0.000	0.700	1.496	0.933	1.300
a	2.649×10^9	1.396	0.000	0.014	0.700	1.995	0.700	0.8000
b	3.584×10^9	0.693	-3.196×10^{-10}	0.000	0.679	0.494	1.403	0.8124
c	5.262×10^9	0.239	0.000	0.000	0.633	0.129	1.857	8.535
d	2.689×10^{10}	0.239	0.000	0.000	0.633	0.129	1.857	8.535
a	2.834×10^9	1.396	0.000	0.000	0.700	1.995	0.700	1.000
b	3.157×10^9	0.740	-7.591×10^{-10}	0.000	0.680	0.546	1.356	0.9228
c	4.336×10^9	0.243	-1.247×10^{-12}	0.000	0.632	0.131	1.853	10.18
d	2.523×10^{10}	0.243	0.000	0.000	0.632	0.131	1.853	10.18
a	3.122×10^9	1.396	0.000	0.000	0.699	1.995	0.700	1.300
a	2.068×10^9	1.445	0.000	0.174	0.700	1.496	0.966	0.8000
b	3.255×10^9	0.813	-8.057×10^{-10}	0.000	0.685	0.508	1.599	0.9928
c	4.300×10^9	0.252	-3.583×10^{-12}	0.000	0.641	0.117	2.160	13.57
d	4.335×10^9	0.252	0.000	0.000	0.641	0.117	2.160	13.57
a	2.449×10^9	1.445	0.000	0.000	0.700	1.496	0.966	1.000
b	2.864×10^9	0.865	-1.578×10^{-9}	0.000	0.684	0.559	1.546	1.137
c	3.679×10^9	0.257	-1.796×10^{-12}	0.000	0.645	0.119	2.155	16.09
d	3.707×10^9	0.257	0.000	0.000	0.645	0.119	2.155	16.09
a	2.662×10^9	1.445	0.000	0.000	0.700	1.496	0.966	1.300
b	2.759×10^9	0.918	-6.128×10^{-9}	0.000	0.684	0.615	1.493	1.373
c	3.254×10^9	0.263	-8.057×10^{-13}	0.000	0.646	0.122	2.149	19.69
d	3.278×10^9	0.263	0.000	0.000	0.646	0.122	2.149	19.69
a	2.174×10^9	1.445	0.000	0.130	0.700	1.995	0.724	0.8000
b	3.640×10^9	0.707	-4.192×10^{-10}	0.000	0.680	0.483	1.463	0.8300
c	5.065×10^9	0.241	0.000	0.000	0.631	0.125	1.929	9.173
d	2.634×10^{10}	0.241	0.000	0.000	0.631	0.125	1.929	9.173
a	2.480×10^9	1.445	0.000	0.000	0.700	1.995	0.724	1.000
b	2.848×10^9	0.752	-8.036×10^{-10}	0.000	0.680	0.531	1.417	0.9464
c	3.960×10^9	0.245	-6.654×10^{-13}	0.000	0.634	0.127	1.925	10.91
d	4.015×10^9	0.245	0.000	0.000	0.634	0.127	1.925	10.91

continued to next paper

Table A1. –continued.

	t_1 (yr)	M_1 (M_\odot)	\dot{M}_1 ($M_\odot \text{yr}^{-1}$)	X_H^c	X_H^s	q	M_2 (M_\odot)	P (days)
a	2.694×10^9	1.445	0.000	0.000	0.700	1.995	0.724	1.300
b	2.732×10^9	0.795	-5.005×10^{-9}	0.000	0.681	0.578	1.375	1.143
c	3.284×10^9	0.251	0.000	0.000	0.632	0.131	1.919	13.39
d	3.319×10^9	0.251	0.000	0.000	0.632	0.131	1.919	13.39
a	1.701×10^9	1.496	0.000	0.231	0.700	1.496	1.000	0.8000
b	3.091×10^9	0.825	-8.864×10^{-10}	0.000	0.685	0.494	1.671	1.022
c	4.056×10^9	0.254	-4.564×10^{-12}	0.000	0.641	0.113	2.243	14.56
d	4.087×10^9	0.254	0.000	0.000	0.641	0.113	2.243	14.56
a	2.162×10^9	1.496	0.000	0.000	0.700	1.496	1.000	1.000
b	2.544×10^9	0.890	-1.750×10^{-9}	0.000	0.685	0.554	1.606	1.147
c	3.308×10^9	0.259	-1.861×10^{-12}	0.000	0.646	0.116	2.237	17.26
d	3.335×10^9	0.259	0.000	0.000	0.646	0.116	2.237	17.26
a	2.324×10^9	1.496	0.000	0.000	0.700	1.496	1.000	1.300
b	2.437×10^9	0.957	-5.621×10^{-9}	0.000	0.686	0.622	1.539	1.363
c	2.919×10^9	0.265	-2.269×10^{-12}	0.000	0.646	0.119	2.231	21.12
d	2.942×10^9	0.265	0.000	0.000	0.646	0.119	2.231	21.12
a	1.781×10^9	1.496	0.000	0.199	0.700	1.995	0.750	0.8000
b	3.674×10^9	0.723	-4.551×10^{-10}	0.000	0.682	0.474	1.523	0.8468
c	4.981×10^9	0.242	-1.567×10^{-13}	0.000	0.630	0.121	2.004	9.854
d	2.594×10^{10}	0.242	0.000	0.000	0.629	0.121	2.004	9.854
a	2.174×10^9	1.496	0.000	0.000	0.700	1.995	0.750	1.000
b	2.549×10^9	0.772	-8.777×10^{-10}	0.000	0.682	0.524	1.474	0.9587
c	3.593×10^9	0.247	-1.763×10^{-12}	0.000	0.635	0.124	1.999	11.70
d	3.635×10^9	0.247	0.000	0.000	0.635	0.124	1.999	11.70
a	2.347×10^9	1.496	0.000	0.000	0.700	1.995	0.750	1.300
b	2.407×10^9	0.824	-4.119×10^{-9}	0.000	0.682	0.579	1.422	1.142
c	2.971×10^9	0.253	-7.284×10^{-12}	0.000	0.633	0.127	1.993	14.36
d	3.004×10^9	0.253	0.000	0.000	0.633	0.127	1.993	14.36
a	1.425×10^9	1.549	0.000	0.289	0.700	1.496	1.035	0.8000
b	2.985×10^9	0.845	-1.021×10^{-9}	0.000	0.686	0.486	1.739	1.039
c	3.841×10^9	0.255	-6.397×10^{-13}	0.000	0.638	0.110	2.329	15.66
d	3.870×10^9	0.255	0.000	0.000	0.638	0.110	2.329	15.66
a	1.890×10^9	1.549	0.000	0.057	0.700	1.496	1.035	1.000
b	2.297×10^9	0.903	-2.169×10^{-9}	0.000	0.686	0.537	1.681	1.178
c	2.954×10^9	0.261	-1.435×10^{-12}	0.000	0.643	0.112	2.323	18.54
d	2.979×10^9	0.261	0.000	0.000	0.643	0.112	2.323	18.54
a	2.060×10^9	1.549	0.000	0.000	0.700	1.496	1.035	1.300
b	2.180×10^9	0.974	-6.159×10^{-9}	0.000	0.687	0.605	1.610	1.389
c	2.625×10^9	0.267	-2.597×10^{-12}	0.000	0.645	0.115	2.317	22.68
d	2.646×10^9	0.267	0.000	0.000	0.645	0.115	2.317	22.68
a	1.496×10^9	1.549	0.000	0.260	0.700	1.995	0.776	0.8000
b	3.728×10^9	0.734	-5.001×10^{-10}	0.000	0.682	0.461	1.591	0.8730
c	4.870×10^9	0.244	-8.408×10^{-13}	0.000	0.625	0.117	2.081	10.61
d	4.927×10^9	0.244	0.000	0.000	0.625	0.117	2.081	10.61
a	1.973×10^9	1.549	0.000	0.000	0.700	1.995	0.776	1.000
b	2.251×10^9	0.783	-1.113×10^{-9}	0.000	0.683	0.508	1.542	0.9872
c	3.117×10^9	0.249	0.000	0.000	0.631	0.120	2.076	12.59
d	3.155×10^9	0.249	0.000	0.000	0.631	0.120	2.076	12.59
a	2.077×10^9	1.549	0.000	0.000	0.700	1.995	0.776	1.300
b	2.150×10^9	0.843	-3.834×10^{-9}	0.000	0.683	0.569	1.482	1.158
c	2.681×10^9	0.255	0.000	0.000	0.631	0.123	2.070	15.41
d	2.711×10^9	0.255	0.000	0.000	0.631	0.123	2.070	15.41